International Journal of Environmental Science and Technology (2024) 21:7615–7630
https://doi.org/10.1007/s13762-024-05506-x

ORIGINAL PAPER

Water remediation using mesoporous silica monolith nanocomposites functionalized with Prussian blue

A. A. Markeb[1] · K. Abdelhameed[1] · W. A. El-Said[1] · N. A. El-Maali[1]

Received: 19 December 2022 / Revised: 7 February 2024 / Accepted: 11 February 2024 / Published online: 15 March 2024

Abstract

A simple, one-pot method was designed for preparing nanocomposite material and its potential applications for water remediation. X-ray diffraction, Fourier Transform infrared, scanning, and transmission electron microscopy, thermogravimetric analysis and derivative thermogravimetry, and N_2 adsorption and desorption isotherm techniques were used to examine the chemical and physical characteristics of the prepared nanomaterials. The developed nano-sized sorbent has a good surface area of about 106.788 $m^2\ g^{-1}$. The synthesized nanocomposite was employed as a sorbent to remove several heavy metals, such as Cd(II), Cu(II), Fe(III), Pb(II), Mn(II), and Cr(VI), and different pesticides (e.g., Diazinon, Parathion Methyl, Malathion, Parathion ethyl, Epoxide, DDE, Dieldrin, and Aldrin). The removal efficiencies were found to be in the range of 9.52–94.8%, 23.14–99.40%, and 8.91–85.50% for pesticides, heavy metals, and physical contaminants, respectively. In addition, the sorption capacities of the different metals ranged from 2.31 to 9.94 mg g^{-1}, and from 2.67 to 28.00 mg g^{-1} for different pesticides. While it was 31.49–306.63 mg g^{-1} for physical contaminants.

Keywords Prussian blue/silica nanocomposites · Heavy metals · Pesticides · Physical contaminants · Adsorption · UV–vis spectroscopy · Atomic absorption

Introduction

Water quality is necessary for humankind's continued existence on the planet. However, the ongoing deterioration of water quality is due to the introduction of significant volumes of contaminants into water bodies because of fast industrialization (Shannon et al. 2008; Qu et al. 2013). Also, the rapid increase in the population, industrialization, and urbanization results in high pollution levels. Around 80% of the world's population faces water supply and security threats. Thus, the development of water remediation methods has got an increasing concern. Drinking water sources may contain several organic and inorganic pollutants. The high levels of these pollutants could cause a high risk of a range of diseases, including gastrointestinal illness, developmental effects, endocrine disruption, and cancer (Kumar and Xagoraraki 2010; Agency 2008; Survey 2010). For instance, pesticides are examples of organic pollutants, which could enter the sources of drinking water or groundwater from agricultural areas or abandoned wells on farms (Agency 2011). Although the human bodies need traces of some heavy metals such as copper, selenium, and zinc to maintain the metabolism. However, human exposure to high concentrations of heavy metals is a big issue due to their poisoning behavior. Heavy metals drinking-water contamination, emission sources into the air, or the intake into the food chain (Yousif et al. 2015; Long et al. 2021a). The dangers of heavy metals are related to their tendency to bioaccumulate and their difficulty to break down or be excreted outside the human body. The toxic effects of heavy metals could result in serious diseases such as reduced growth, organ damage (liver and kidney), nervous system damage, cancer, and even death (Liu et al. 2019; Farah et al. 2012a; Miao et al. 2007). Water contamination is a worldwide problem that needs an ongoing examination of water quality. Therefore, removing heavy metals as well as other contaminants of emerging concerns from water is urgently needed (Lin et al. 2010). Thus, various techniques have been reported for expelling heavy metals from water, which incorporate substance

Editorial responsibility: Q. Aguilar-Virgen.

✉ W. A. El-Said
awaleedahmed@yahoo.com

[1] Chemistry Department, Faculty of Science, Assiut University, Assiut 71516, Egypt

precipitation, coagulation, flocculation, invert osmosis, adsorption, and filtration. However, these methods have some disadvantages including higher cost and lower efficiency. The removal of heavy metals based on metal adsorption by using the mass exchange system is an outstanding technique (Miao et al. 2007) because of its simplicity and low-cost advantages (Zhang et al. 2004).

Nanomaterials have been applied in many environmental applications such as pollutant sensing, catalytic environmental contaminants treatment, and removal (El-Din et al. 2018; El-Said et al. 2018; Alsulami et al. 2022). Also, nanomaterials were used for pesticide remediation, as chelating agents for a polymer to enhance the ultrafiltration process and drinking water purification. A blue dye known as Prussian blue (PB) is also an artificial peroxidase. Iron (III) chloride and potassium ferrocyanide interact to form PB, a type of metal hexacyanoferrate. PB is composed of a potassium ferrous ferricyanide hexacyano hexahydrate $Fe_4III[FeII(CN)_6]_3$ repeating unit and a mixed-valent iron cyanide complex (Adekunle et al. 2012; Haghighi et al. 2010; Li et al. 2007). However, PB and its analogs have unique properties such as electrochromic, electrochemical, photophysical, magnetic, and properties among others (Farah et al. 2012b; Cui et al. 2012; Zhang et al. 2009). The present work aims to: (1) synthesize the PB/silica monolith (HOM) at nanoscale size using a one-pot synthetic method, (2) utilize the PB/silica HOM nanocomposite as a sorbent to remove various contaminants, such as pesticides and heavy metals and (3) to assess the effectiveness of the synthesized sorbent in removing various pollutants from aqueous solutions through the removal efficiency and adsorption capacity parameters.

Materials and methods

Materials

All materials were used as tetraethyl orthosilicic acid (TEOS, 99.9 percent). Pluronic F-127, aluminum nitrate, lead nitrate, copper nitrate, iron nitrate, manganese nitrate, cadmium nitrate, calcium nitrate, ethanol, phosphoric acid, ferric chloride, sodium citrate, potassium ferrocyanide, organochlorine, and organophosphate pesticides, potassium dichromate, 1,5-diphenylcarbazide indicator, acetone, phosphoric acid, sodium hydroxide were purchased from Sigma-Aldrich, Germany, with an essay ≥ 99%.

Synthesis of Prussian Blue/silica monolith (HOM) nanocomposites

The PB/silica HOM nanocomposites sorbent was created using the conventional solgel method. In summary, 11.07 g of pluronic F-127 and 16.06 g of TEOS were combined in a flask. Next, a rotatory evaporator was used to dissolve the mixture and cod it as a solution (1). Then, 2.5 g of $FeCl_3$, 5.28 g of potassium ferrocyanide, and 1.62 g of sodium citrate were dissolved separately in 40 mL of distilled water. Then, 20 mL of each solution was added to the solution (1). Leave it in the rotatory evaporator for 15 min. Add to this mix about 10 ml of H_3PO_4 at pH = 1.6 until dissolved and leave it in the rotatory evaporator for 15 min. Heat at 80 °C to evaporate the water and ethanol wash using ethanol first and then distilled water. Finally, dry at 60 °C overnight.

Characterization

The synthetic PB/silica HOM nanocomposites' FTIR spectrum was measured in KBr pellets using a Nicolet Spectrophotometer, model 6700 (USA), in the range 4000–400 cm^{-1} with a resolution of 4 cm^{-1} and 16 scans. The surface morphologies were analyzed with scanning electron microscopy (SEM), which stands for scanning electron microscope (JEOL JSM-5400 LV, Japan). Using a fine-coat ion sputtering apparatus (JEOL JTC-1100E, Japan), the gold film was applied to the samples while they were at room temperature. Moreover, the size of PB/silica HOM nanocomposites was achieved using a High-resolution transmission electron microscope (HR-TEM) (FEI^{TM}TECNAI G^2 spirit TWIN,

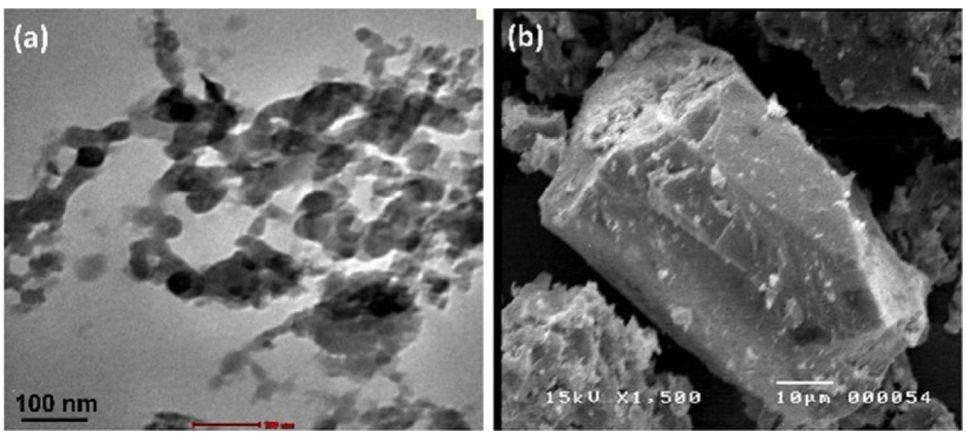

Fig. 1 **a** TEM image of PB/silica HOM nanocomposites, and **b** SEM image of PB/silica HOM nanocomposites

Model No. 9432 050 18,111, Czech Republic) conducted by VELETA Camera at an accelerating voltage of 120 kV. PB/silica HOM nanocomposites' textural characteristics were assessed using a BELSORP MIN-II analyzer using nitrogen adsorption at 77 K. (MicrotracBEL Corp., Osaka, Japan). The Shimadzu was used to acquire the TGA/DTG analyses. DTG-60H thermogravimetric, under an N_2 atmosphere (Shimadzu, Kyoto, Japan). Using a Philips PW 1710 X-ray diffractometer with nickel-filtered CuKα radiation ($\lambda = 1.54060$ Å) and running at 40 kV and 40 mA, particle size in the 4–90° range was examined, and finally, by

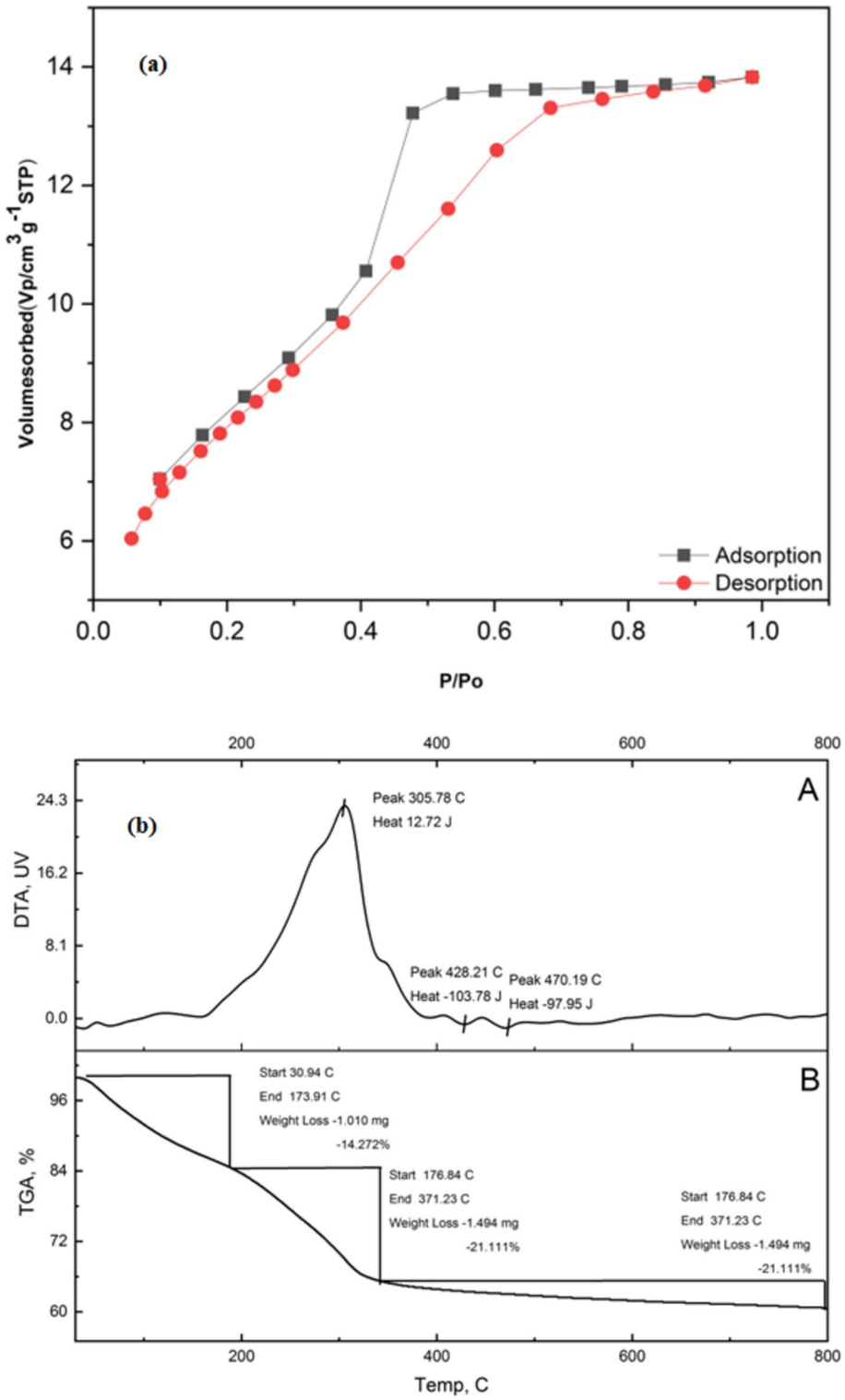

Fig. 2 N_2 sorption/desorption isotherms of PB/silica HOM nanocomposites, and **b** Thermogravimetric analysis (TGA) of PB/silica HOM nanocomposites

utilizing a calibration curve to quantify metal ions using atomic absorption (Contr AA700, Germany).

Adsorption experiments

PB/silica HOM nanocomposites sorbent in each quantity (1 g L^{-1}) was mixed with a volume of solution containing different water contaminants with an initial concentration of C_o. For 24 h, the flask was kept agitated at 25 °C. The sorption capacity (q_{eq}, mg(M) g^{-1} (PB/silica HOM nanocomposites)) and the removal efficiency (RE%) utilizing Eqs. (1) and (2), respectively, were calculated (Long et al. 2021a):

$$Q = \left(C_i - C_e\right)V/m \tag{1}$$

$$\text{RE}\ \% = \left(C_i - C_e\right)/C_i x\, 100 \tag{2}$$

where m represents the mass of the adsorbent in grams within the reaction mixture, V is the reaction mixture's volume in liters, C_i is the metallic ion's initial concentration (mg L^{-1}), and C_e is the equilibrium concentration (mg L^{-1}) (Liu et al. 2019; Farah et al. 2012a).

Metal ions sorption and detection

Lead, cadmium, copper, manganese, and iron are among the heavy metal pollutants being investigated. The sorption testing was conducted in batch mode. Typically, a fixed amount of sorbent, PB/silica HOM nanocomposites, and 50 mL of an aqueous solution was combined with 50 mg of an individual containing Cd(II), Cu(II), Fe(III), Pb(II), Mn(II) and Cr(VI) at a concentration of 10 mg L^{-1} for C_o (sorbent dosage, SD: 1 g L^{-1}). Using NH_4OH solutions, the solution's pH was initially adjusted to 7.15. For 24 h, the flask was kept agitated at 25 °C. Filtration was used to separate the solution from the sorbent. Atomic absorption was used to determine the residual metal ion concentration (C_{eq}, mg L^{-1}), after which the sorption capacity (q_{eq}, mg g^{-1}) and removal efficiency (RE%) were estimated and UV–vis for determining the residual metal ion concentration (C_{eq}, mg L^{-1}) of Cr(VI).

Detection and sorption of pesticides

Pesticide sorption tests were run in batch mode. Typically, a volume of pesticide combination solution was combined with a predetermined amount of sorbent PB/silica HOM nanocomposites, 50 mg (50 mL) containing organochlorine pesticides (HCB, Lindane, Epoxide, DDE, Dieldrin, and Aldrin), organophosphorus pesticides (Diazinon, Disulfaton, Parathion Methyl, Malathion, and Parathion Ethyl), and Trifluraline initially had a pH of 7.15 that was raised using NH_4OH solutions. For 24 h, the flask was kept agitated at 25 °C. Filtration was used to separate the solution from the sorbent. Then, the residual concentration of pesticides was determined by extraction of the pesticides in the filtrate with 2 mL of n-Hexane, followed by shaking for 2 min, leaving

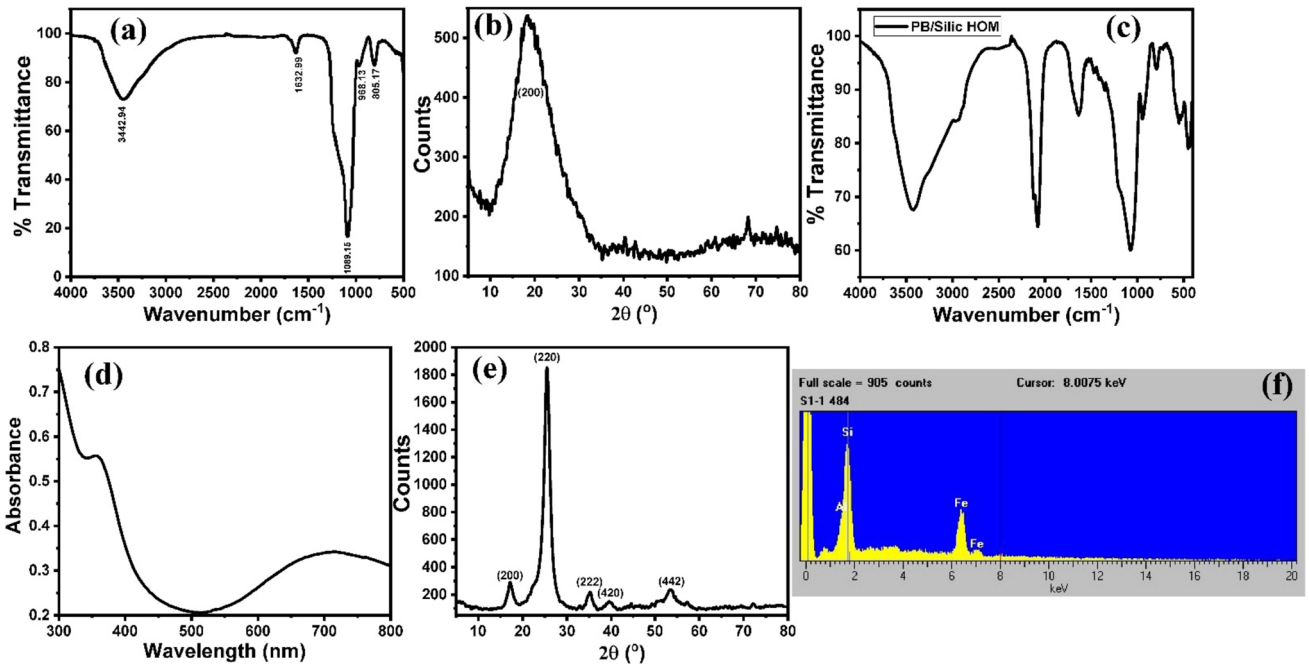

Fig. 3 **a** FT-IR spectrum of silica NPs, **b** XRD Pattern of silica NPs, **c** FT-IR spectrum of PB/silica HOM nanocomposites, **d** UV–visible spectrum of PB/silica HOM nanocomposites, **e** XRD Pattern of PB/silica HOM nanocomposites, and **f** EDX analysis of the PB/silica HOM nanocomposites

it for 8 min to separate the two layers, and withdrawing the organic layer in a glass vial for injection. Gas chromatography–mass spectrometry was used to examine the residual pesticide content (C_{eq}, mg L^{-1}), and the sorption capacity and removal efficiency (RE%) were calculated.

Physical contaminants removal

The physical pollutants being examined are total solids, total dissolved solids, total suspended solids, and electrical conductance. Briefly, a fixed amount of sorbent PB/silica HOM nanocomposites, (50 mg) was combined with a certain volume of tap water. 50 mL, withdrawn from the drinking water source of Assiut University, Egypt, at concentration C_o: mg L^{-1} (sorbent dosage, 1 g L^{-1}). The sample of tap water had a pH of 7.15. The flask was then kept agitated for 24 h at 25 °C. The solution was left for settling, then 25 mL of the sample was withdrawn to determine the residual concentration (C_{eq}, mg L^{-1}), followed by analysis using a conductivity meter (JENWAY, model 4510, Made in EU). The sorption capacity (q_{eq}, mg g^{-1}) and removal efficiency (RE%) were estimated. The Spectro UV–vis Dual-Beam PC Scanning Spectrophotometer UVD-2950 (Made in the U.S.A).

Results and discussion

Characterization of the synthesized nanomaterials

The physical structure and chemical composition of the PB/silica HOM nanocomposites was characterized using a variety of techniques.

Morphology of sorbent—SEM and TEM observations

The surface of nanoporous PB/silica HOM nanocomposites was characterized using HR-TEM and SEM analysis (Fig. 1a and b). The hollow, spherical, porous structure of the sorbent is visible in the HR-TEM, which also supports its presence. Figure 2a shows the TEM image of PB/silica HOM nanocomposites, which illustratesthe formation of high-dimensioned aggregates of NPs without a defined shape (Shannon et al. 2008). The surface morphology of PB/silica HOM nanocomposites is shown in Fig. 1b using SEM. The results showed the formation of large particles (micro size) in addition to the presence of tiny particles (nano size) on the surface of the large particles.

Textural characteristics of the sorbent – BET analysis

Using the N_2 adsorption/desorption method, the sorbent, PB/silica HOM nanocomposites' textural properties were obtained. The BET-surface area (SA), BJH pore volume (Vp), and average pore diameter (Dp) were computed, as illustrated in Fig. 2a. The SA is approximately 167.246 $m^2 g^{-1}$ when Langmuir is used. While the volume of porous material is roughly 0.082 $cm^3 g^{-1}$. The N_2 adsorption/desorption isotherm shows the classic IV type, which has a protracted hysteresis loop at low P/Po (in the range of 0.20–1.00). This finding indicates the existence of micropores in PB/silica HOM nanocomposites. The primary porous volume has a uniform pore diameter of 1.54 nm because of capillary evaporation and the isotherm's steepness; nevertheless, inter-sphere holes cause another pore size that is near 24 nm, as observed by the TEM study. According to this

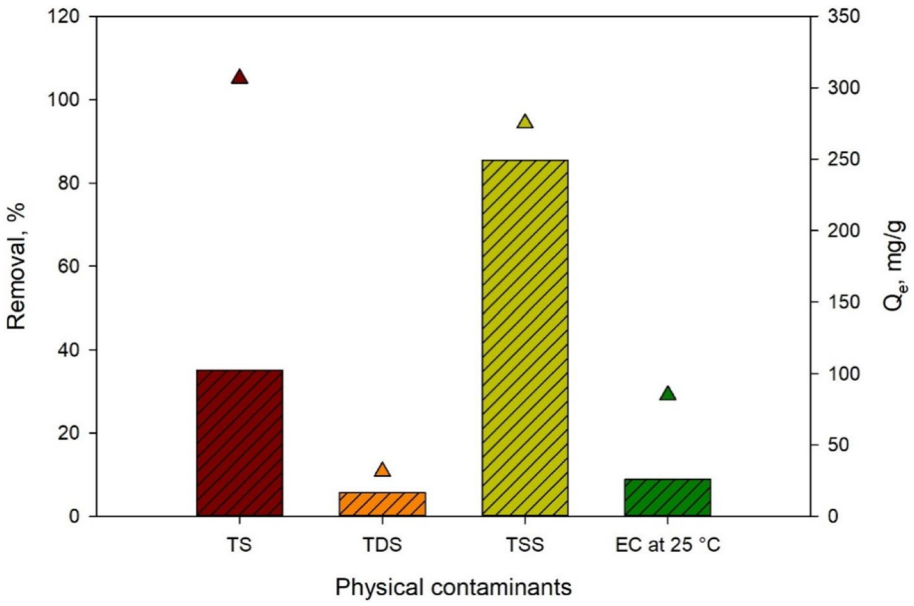

Fig. 4 Physical Contaminants removal with PB/silica HOM nanocomposites

investigation, interconnected hollow microspheres are what give the sorbent its high porosity and specific surface area.

Thermogravimetric analysis

The thermogravimetric analysis (TGA) profile of the PB/silica HOM nanocomposites is presented in Fig. 2b. To check the developed PB/silica HOM nanocomposite's thermal stability, TGA analysis was used. The most common method for assessing through TGA of weight loss, nanoparticle presence in nanomaterials is discovered. It is challenging to interpret these curves because catalyst particles are present during the weight loss analysis. The stability of the PB/silica HOM nanocomposites is determined by the temperature at which they oxidize. The TGA graph depicts three places where the PB/silica HOM nanocomposites' weight has decreased. In Fig. 2b(A). The thermogram shows three identified areas of weight reduction. The elimination of water molecules that were intrinsically absorbed in the PB/silica HOM nanocomposites and started at about 30.94 °C and ended at 173.91 °C may be the primary factor in the initial weight loss. The presence of soluble and insoluble PB nanoparticles may have contributed to the second and final weight losses, which were between 176.84 °C and 371.23 °C and 374.16 °C and 794.72 °C, respectively (Qu et al. 2013). Water loss from the PB/silica HOM nanocomposite structure was attributed to the mass drop (14.272%) in step I. According to TG, there are four water molecules per PB/silica HOM nanocomposites molecule. The mass losses found in stages II (21.111%) and III (3.589%) primarily reflect cyanide

Table 1 Method validation parameters for pesticide determination using GC/MS the synthesized nanocomposite

Analyte	Linearity	Reportable range (μg L^{-1})	Accuracy (R, %)	Precision (RSD, %)	Estimated Detection limit (μg L^{-1})	Limit of quantitation (μg L^{-1})	Method Detection limit (μg L^{-1})
Diazinon	0.9962	0.06–7.68	99.32	4.77	0.205	0.189	0.059
Aldrin	0.9945	0.06–7.68	82.99	6.89	0.060	0.171	0.054
Dieldrin	0.9941	0.06–7.68	93.86	2.14	0.147	0.171	0.054
DDE	0.9951	0.06–15.36	100.64	0.77	0.070	0.174	0.055
Epoxide	0.9959	0.06–7.68	97.80	0.37	0.108	0.002	0.001
Parathion ethyl	0.9954	0.06–7.68	99.54	25.10	0.320	0.692	0.218
Parathion Methyl	0.9996	0.06–7.68	93.24	1.78	0.204	0.186	0.058
Malathion	0.9986	0.06–7.68	97.39	5.81	0.219	0.178	0.056

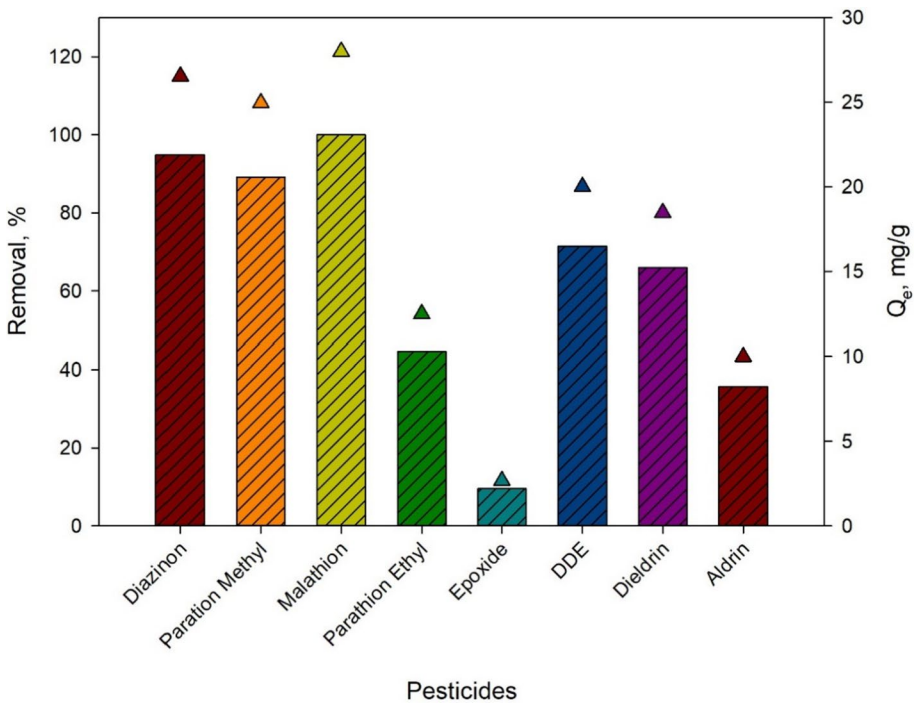

Fig. 5 Pesticides removal with PB/silica HOM nanocomposites

groups being released from the PB/silica HOM nanocomposites structure. In step III, nitrogen is released in addition to $(CN)_2$ emissions. (Fig. 2b(B)).

FTIR analysis

Figure 3a shows the Fourier transform infrared (FTIR) spectrum of the monolithic silica NPs. The spectrum showed an absorption band at 344.9 cm^{-1}, which is attributed to the stretching mode of Si–O–H and H_2O (absorbed water molecules), 1189 cm^{-1} (s, Si–O–Si), and 805 cm^{-1} (m, Si–OH). Furthermore, the PB/silica HOM nanocomposites' FTIR spectrum was given (Fig. 3c). The stretching vibration of the CN group in potassium ferricyanide is responsible for the prominent peak at 2081.92 cm^{-1} which is the typical absorption peak of PB/silica HOM nanocomposites. The absorption bands between 3358.71 and 1606.51 cm^{-1}, which are attributed to the O–H stretching mode and H–O–H bending mode, respectively, demonstrate the presence of interstitial forces of attraction in the sample. Because of the structure of the Fe^{2+}-CN-Fe^{3+} connection in PB/silica HOM nanocomposites, the absorption bands at 606.78 cm^{-1} are caused by this (Kumar and Xagoraraki 2010; Agency 2008; Survey 2010).

Spectrophotometric analysis

The PB/silica HOM nanocomposites' spectra show a prominent absorption peak at 700 nm, which is related to the strong charge transfer absorption band brought on by the Fe^{2+}-CN-Fe^{3+} polymeric sequence of PB (Fig. 3d) (Agency 2008, 2011).

X-Ray Diffraction analysis

By using an X-ray diffraction (XRD) approach that relies on the elastic scattering of X-rays from structures with long-range order, XRD can determine the geometry or form of a molecule. The XRD pattern of the silica NPs (Fig. 3b) showed a broad peak that revealed the amorphous nature of

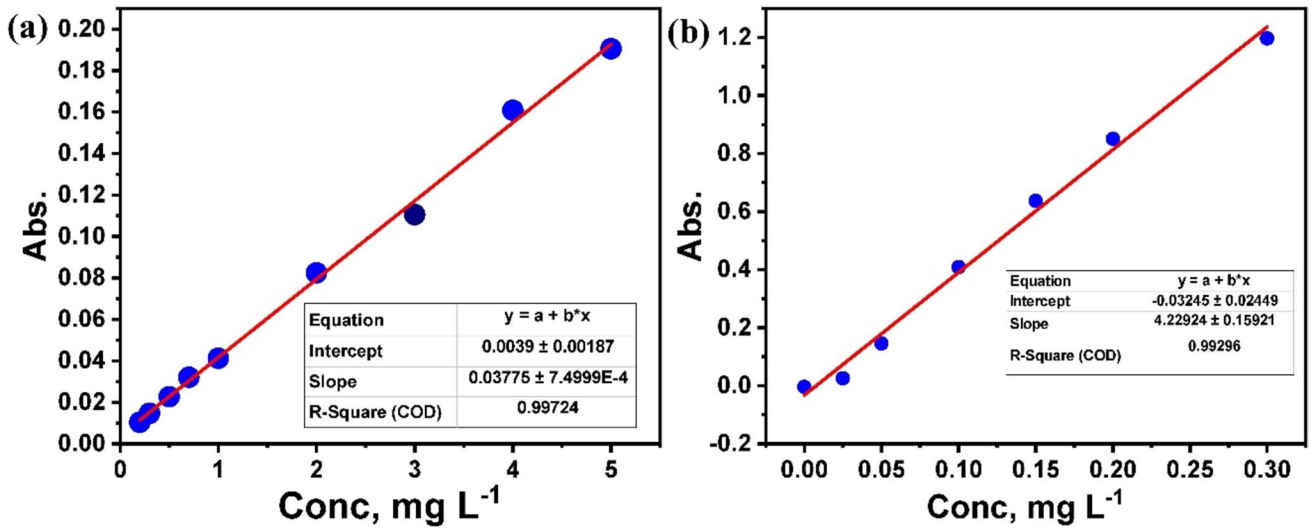

Fig. 6 Calibration curve of lead by **a** Atomic absorption and **b** UV–vis

Table 2 Method validation parameters for heavy metals determination

Analyte	Linearity	Reportable range (mg L^{-1})	Accuracy (R, %)	Precision (RSD, %)	Estimated Detection limit (mg L^{-1})	Limit of quantitation (mg L^{-1})	Method Detection limit (mg L^{-1})
Lead	0.9970	0.000–5.000	86.69	5.97	0.056	0.309	0.097
Cadmium	0.9960	0.100–1.000	98.95	2.70	0.006	0.076	0.024
Copper	0.9988	0.000–5.000	108.88	1.71	0.018	0.266	0.084
Manganese	0.9950	0.300–3.000	96.77	2.78	0.067	0.103	0.329
Iron	0.9990	0.300–3.000	105.24	4.85	0.100	0.801	0.252
Chromium (VI)	0.9990	0.001–0.500	101.52	2.37	0.001	0.011	0.003

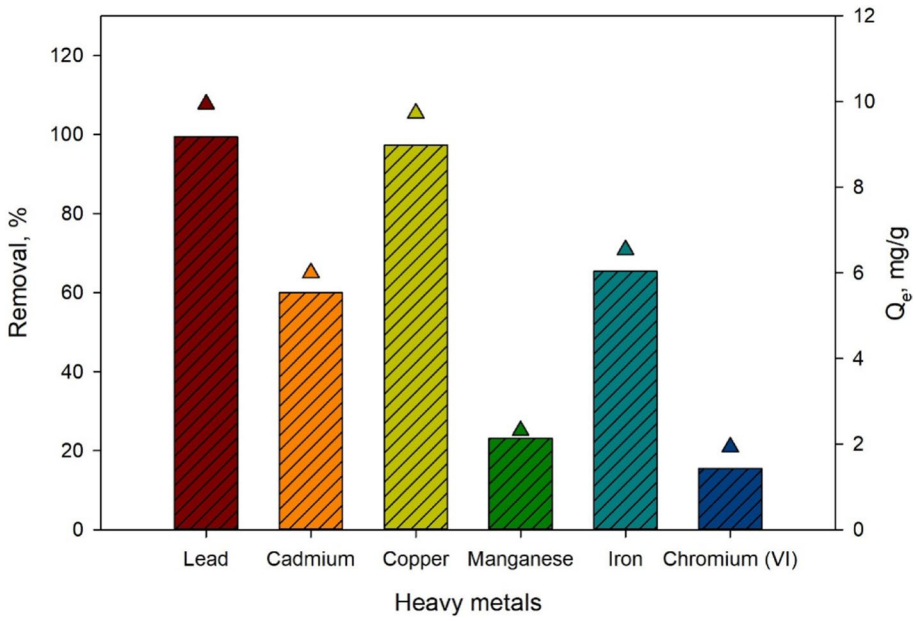

Fig. 7 Metal ions removal using PB/silica HOM nanocomposites

the fabricated silica NPs. The pattern of the PB/silica nanocomposites showed diffraction peaks at 17.200°, 25.519°, 35.260°, 39.460°, and 53.680°, which can be allocated to the Prussian blue phase (200, 220, 222, 420, and 442) crystal planes, respectively, as shown in Fig. 3e. These peaks can be connected to the face-centered cubic PB with space group structure Fm3m (Survey 2010).

Energy dispersive X-ray (EDX) analysis of PB/silica HOM nanocomposites

Finally, the EDX analysis was used to study the chemical composition of the fabricated PB/silica HOM nanocomposites. Figure 3f shows the EDX spectrum of PB/silica HOM nanocomposites, which confirmed the presence of the Si, Fe, and Al elements with high concentrations of Si elements. The results confirmed the fabrication of a highly pure composite.

Contaminants removal screening

Physical contaminants removal

The sorption capacity (q_{eq}) and the removal efficiency (RE%) for physical contaminants such as TS, TDS, TSS, and EC are illustrated in Fig. 4. It was found that the REs% are 35.11%, 5.71%, 85.50%, and 8.91%. for TS, TDS, TSS, and EC, respectively. Also, the values of Q_e were found to be 306.63 mg g^{-1}, 31.49 mg g^{-1}, 275.16 mg g^{-1}, and 84.96 mg g^{-1} for TS, TDS, TSS, and EC, respectively.

Pesticides removal

The contaminated water was separated from the sorbent by filtration. Then, the residual concentrations in the aqueous solutions that contain the different pesticides were determined by GC/MS. Thus, technique validation is carried out to show that the method is appropriate for the intended use. All steps in the method validation process: specificity, accuracy, linearity, precision, range, detection limit, quantitation limit, and robustness are validated using reference materials because the main difficulty in doing so is that only reference materials with well-characterized properties and well-documented purities should be used during method

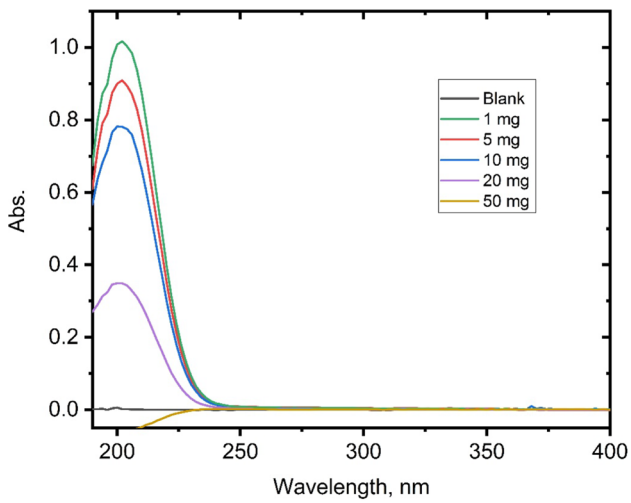

Fig. 8 The effect of adsorbent dose on the removal of 100 mg L^{-1} Pb(II) ions

Table 3 Comparison of pesticides sorption capacities of our work with other sorbents found in the literature

Analyte	Adsorbent	Adsorption capacity (mg g^{-1}) [reference]	Analyte	Adsorbent	Adsorption capacity (mg g^{-1}) [reference]	Analyte	Adsorbent	Adsorption capacity (mg g^{-1}) [reference]
Diazinon	Sn-MOF	587.39 (Alrefaee, et al. 2023)	**Dieldrin**	Triolein embedded	0.002 (Ru et al. 2007)	**Parathion Methyl**	β-Cyclodextrin/ Zeolite	194.7 (Abukhadra et al. 2022a)
	Ca-montmorillonite	9.5 (Kabwadza-Corner et al. 2014)		Al30/bentonite	0.191 (Farghali et al. 2020)		Fe0@Chitosan/Cellulose	(107.6 (Abukhadra et al. 2022b)
	Nanocrystalline MgO	20 (Armaghan and Amini 2017)		GO-MNPs	1.0 (Shrivas et al. 2017)		BSA/PCN-222(Fe)	370.4 (Sheikhi et al. 2021)
	Magnetic guar gum	47.17 (Nikzad et al. 2019)		Montmorillonite Clays	171.41 (Hearon et al. 2020)		PB/silica HOM nanocomposites	24.96 [Our Work]
	Acid treated zeolite	15.1 (Gunasekara et al. 2008)		PB/silica HOM nanocomposites	18.47 [Our Work]	**Malathion**	Kaolin	2.80 (Pal and Vanjara 2001)
	Activated coconut shell biochar	9.65 (Baharum et al. 2020)	**DDE**	poly(HEMA-MAsp) cryogels	31.51 (Köse and Köse 2017)		TTA-K	5.85 (Pal and Vanjara 2001)
	Chitosan/Carbon nanotube	222.86 (Firozjaee et al. 2017)		BAGASSE FLY ASH,	0.0020 (Gupta and Ali 2001)		Montmorillonite	7.95 (Pal and Vanjara 2001)
	Pumice	20.65 (Dehghani et al. 2021)		DMG composite	10.06 (Sanad et al. 2023)		DTA-M	10.50 (Pal and Vanjara 2001)
	Spherical SBA-15	476.1 (Ahmadian and Anbia 2021)		HMS silica	0.024 (Sawicki and Mercier 2006)		TTA-M	12.60 (Pal and Vanjara 2001)
	PB/silica HOM NPs	26.54 [Our Work]		CD-HMS-2%	0.025 (Sawicki and Mercier 2006)		CP-M	14.20 (Pal and Vanjara 2001)
Aldrin	Patellidae Shells	111.63 (Bakka et al. 2018)		CD-HMS-4%	0.007 (Sawicki and Mercier 2006)		Bentonite	5.75 (Pal and Vanjara 2001)
	(Chi-EDGE-Fe)	74.84 (Rosales et al. 2021)		PB/silica HOM nanocomposites	20.00 [Our work]		TTA-B	16.70 (Pal and Vanjara 2001)
	Clinoptilolite	0.005 (Sprynskyy et al. 2008)	**Parathion ethyl**	To the best of our knowledge, there is no work for its removal by adsorption in the literature			De-Acidite FF-IP	1.25 (Naushad et al. 2013)
	Acid-treated olive stones	19.54 (Bakouri et al. 2009)		PB/silica HOM nanocomposites	12.47 [Our work]		Chitosan-alginate	20.00 (Sabbagh et al. 2021)
	Chitosan beads	2 X 10^{-6} (Lu et al. 2011)					PB/silica HOM nanocomposites	28.00 [Our Work]
	Bacterial cells	20 X 10^{-6} (Mac Rae 1986)						
	Biomimetic absorbent	0.00089 (Liu et al. 2007)						
	Cellulose acetate/ triolein (CA-triolein)	4.00 (Liu et al. 2009)						

Table 3 (continued)

Analyte	Adsorbent	Adsorption capacity (mg g^{-1}) [reference]	Analyte	Adsorbent	Adsorption capacity (mg g^{-1}) [reference]	Analyte	Adsorbent	Adsorption capacity (mg g^{-1}) [reference]
	Q-Fe	74.84 (Rosales et al. 2021)						
	PB/silica HOM nanocomposites	9.98 [Our Work]						

validation activities. The analytical approach showed initial and extended validation for its ability to provide mean recovery values at each spiking level within the range of 70–120 percent and spiked recovery experiments were carried out. A minimum of five replicates are carried out to verify the suggested method's accuracy. Table 1 provides an overview of the Method Detection Limit (MDL) and Limit of Detection (LOD) for the lead under examination. To ensure that the procedure is reliable, data reproducibility is verified under typical circumstances. So, method validation parameters are shown in Table 1. In addition, the sorption capacity (q_{eq}) and the removal efficiency (RE %) for Diazinon, Parathion Methyl, Malathion, Parathion ethyl, Epoxide, DDE, Dieldrin, and Aldrin are illustrated in Fig. 5. It was found that the RE% is 94.80%, 89.14%, 100%, 44.55%, 9.52%, 71.43%, 65.96%, and 35.64, and the Q_e was found to be 26.54 mg g^{-1}, 24.96 mg g^{-1}, 28.00 mg g^{-1}, 12.47 mg g^{-1}, 2.67 mg g^{-1}, 20.00 mg g^{-1}, 18.47 mg g^{-1}, and 9.98 mg g^{-1} for Diazinon, Parathion Methyl, Malathion, Parathion ethyl, Epoxide, DDE, Dieldrin, and Aldrin, respectively. The reason for the different removal efficiencies of pesticides from aqueous solutions could be attributed to the variation of the hydrophobic and electrostatic interactions between the heterocyclic conjunction of the pesticides and the functional groups.

Heavy metals removal

The determination of heavy metals from the water was evaluated and validated using atomic absorption spectroscopy and UV/Vis spectrophotometric techniques. The correlation coefficients from linearity studies of Pb(II) as an example of heavy metal determination were demonstrated in Fig. 6 using both techniques. Also, the validation parameters for heavy metal determination are presented in Table 2.

Screening of heavy metals removal The sorption capacity (q_{eq}) and the removal efficiency (RE%) for Cd(II), Cu(II), Fe(II), Pb(II), and Mn(II) are illustrated in Fig. 7. It was found that the RE% are 59.97%, 97.33%, 65.39%, 99.4%, and 23.14%, and the Q_e were found to be 6.00 $mg_{(M)}$ g^{-1}, 9.73 $mg_{(M)}$ g^{-1}, 6.54 $mg_{(M)}$ g^{-1}, 9.94 $mg_{(M)}$ g^{-1},2.31 $mg_{(M)}$ g^{-1} and 4.95 $mg_{(M)}$ g^{-1} for Cd(II), Cu(II), Fe(III), Pb(II), Mn(II) and Cr(IV) respectively. The variation in the removal efficiencies of heavy metals could be attributed to the different atomic sizes of the heavy metals as well as the variations in their affinities of heavy metals toward the adsorbent nanocomposites. Additionally, the proposed mechanism of heavy metal removal is ion exchange or complex formation between the functional groups of the adsorbent and the metal ions. The variation of the RE% could be related to

Table 4 Comparison of metals sorption capacities with other sorbents

Analyte	Adsorbent	Adsorption capacity (mg g^{-1}) [reference]	Analyte	Adsorbent	Adsorption capacity (mg g^{-1}) [reference]	Analyte	Adsorbent	Adsorption capacity (mg g^{-1}) [reference]
Cu (II)	Red mud	19.72 (López et al. 1998)	**Cd(II)**	Coffee grounds	15.65 (Azouaou et al. 2010)	**Fe(II)**	nano-biosorbents	222.56 (Zadeh et al. 2022)
	Soybean straw	5.40 (Sciban et al. 2008)		Red mud	10.57 (López et al. 1998)		BFAC	26.15 (Foo et al. 2013)
	Corn stalk	3.75 (Zhu et al. 2017)		Soybean straw	2.02 (Sciban et al. 2008)		CGAC	0.02 (Ching et al. 2011)
	Activated poplar sawdust	9.2 (Acar and Eren 2006)		Corn stalk	5.17 (Zhu et al. 2017)		Resin	59.24 (Víctor-Ortega et al. 2016)
	Spent-activated clay	10.9 (Weng et al. 2007)		Dried sludge	6.6 (Ong et al. 2013)		GAC	3.601 (bin Jusoh, A., W.H. Cheng, W.M. Low, A. Nora'aini, and M.J. Megat Mohd Noor 2005)
	Wheat straw	5.00 (Louis and Proc. 1999)		Nano-γ-Al_2O_3	1.1 (Shokati Poursani et al. 2015)		MMWCNT	197.95 (Alimohammadi et al. 2017)
	Oat straw	5.17 (Louis and Proc. 1999)		Wheat straw	5.17 (Louis and Proc. 1999)		Carbon	57.13 (Moreira et al. 2004)
	Mesoporous silica materials	36.3 11.57 (Zhu et al. 2017)		Oat straw	4.76 (Louis and Proc. 1999)		TiO_2/SiO_2	95.2 (Salimi et al. 2022)
	magnetic Prussian blue	11.2 (Uogintė et al. 2019a)		Mesoporous silica materials	32.3 9.25 (Zhu et al. 2017)		Cinopitlolite modified by 0.1 Hcl	81.53 (Salimi et al. 2022)
	nano-magnetic Prussian blue based on graphene oxide sorbent	138 (Uogintė et al. 2019b)		Magnetic Core–Shell Fe_3O_4@Prussian Blue	9.25 0.89 (Long et al. 2021b)		PB/silica HOM nano-composites	6.54 [Our Work]
	PB/silica HOM nano-composites	9.73 [Our Work]		PB/silica HOM nano-composites	6.00 [Our Work]		Wheat straw	0.88 (Louis and Proc. 1999)

Table 4 (continued)

Analyte	Adsorbent	Adsorption capacity (mg g^{-1}) [reference]	Analyte	Adsorbent	Adsorption capacity (mg g^{-1}) [reference]	Analyte	Adsorbent	Adsorption capacity (mg g^{-1}) [reference]
Pb (II)	Soybean straw	6.84 (Sciban et al. 2008)	**Mn(II)**	TiO_2-based adsorbent	73.83 (Fialova et al. 2023)	**Cr(VI)**	Oat straw	4.29 (Louis and Proc. 1999)
	Corn stalk	6.01 (Zhu et al. 2017)		nano-biosorbents	158.56 (Zadeh et al. 2022)		magnetite nanoparticles	0.015 (Padmavathy et al. 2016)
	Nano-γ-Al_2O_3	6 (Shokati Poursani et al. 2015)		Natural zeolite tuff	10 (Rajic et al. 2009)		poly-(ethylene-co-vinyl alcohol) nanofibers	90.75 (Xu et al. 2015)
	Wheat straw	9.90 (Louis and Proc. 1999)		granular activated carbon	2.5451 (bin Jusoh, A., W.H. Cheng, W.M. Low, A. Nora'aini, and M.J. Megat Mohd Noor 2005)		CTS-Cin	61.35 (Khalil and T., A. Elhusseiny, A. El-Dissouky, and N. Ibrahim 2019)
	Oat straw	18.97 (Louis and Proc. 1999)		tannic acid immobilized activated carbon	1.73 (Üçer et al. 2006)		Fe_3O_4@CTS-Cin	58.14 (Khalil and T., A. Elhusseiny, A. El-Dissouky, and N. Ibrahim 2019)
	Mesoporous silica materials	58.5 18.7 (Zhu et al. 2017)		activated carbon from tire residuals	120 (Niksirat et al. 2019)		α-Fe_2O_3 nanofibers	16.18 (Ren et al. 2013)
	magnetic Prussian blue	39.5 (Uogintė et al. 2019a)		PB/silica HOM nanocomposites	2.31 (our work)		NH_2–ASNs	34.0 (Jang et al. 2020)
	nano-magnetic Prussian blue based on graphene oxide sorbent	443 (Uogintė et al. 2019b)					NH_2–MSNs	42.2 (Jang et al. 2020)
	PB/silica HOM nanocomposites	9.94 [Our Work]					Al-SWTRs	10.9 (Zhou and Haynes 2011)
							PB/silica HOM nanocomposites	4.95 [Our Work]

the different factors that affect the removal ability of the PB adsorbent as follows:

1) The presence of tiny air cavities, which could exhibit a high adsorption capacity based on flotation properties (Feng et al. 2016).
2) The presence of the Fe(II)/Fe(III) redox couple could play a key role in changing the oxidation state of some cations and the deposit of these cations at the surface of the adsorbent (Kim et al. 2022).
3) It is reported that PB works as ion-sieves, which could selectively remove ions based on their ionic radius (Feng et al. 2016; Melo et al. 1994). This could be the reason for the highest RE% of PB toward Pb^{2+} which has the largest ionic radii (Pb^{2+}, 119 pm). While the smallest ion (Mn^{2+}, 70 pm) showed a lower RE%. Thus, it plays the main role in the selectivity of the PB absorbent. The highest removal obtained was found to be 99.4% for Pb(II) ions from water. Hence, the effect of dosage on the removal of Pb(II) was selected to be studied in the next section.

Effect of PB/silica HOM nanocomposites adsorbent dosage on Pb(II) removal Processes for removing Pb(II) are contrasted. In general, a larger number of researchers have investigated a wide range of techniques to remove Pb(II) ions from industrial effluent. These treatment techniques, which can be categorized as chemical, physical, and biological, are frequently used due to their various benefits, including high selectivity separation, ease of control, and reduced space requirements. The best way to treat industrial effluent to remove Pb(II) ions may be through physicochemical processes. Due to the high cost of the chemicals utilized and significant energy consumption, they continue to have high running costs. Adsorption is a promising technique for the simultaneous removal of organic and inorganic contaminants since metal-contaminated wastewater may contain a variety of inorganic and organic substances. Overall, each treatment method has its advantages and limitations. At a pH of 7.15, 20 °C, and an initial concentration of 100 mg L^{-1} of Pb(II), the experiment was carried out. The weight of the adsorbent ranged from 0.001 to 0.050 g. The response of the Pb(II) ion with different PB/silica HOM nanocomposites' doses is shown in Fig. 8. It can be proven that the removal efficiency increases with the weight of the adsorbent. This could be attributed to the increase in adsorption sites on the adsorbent nanocomposites with increasing the amount of the adsorbent. For instance, the higher removal efficiencies were found to be 10.99%, 80.77%, 93.80%, 99.91%, and 100% for adsorbent amounts of 0.001 g, 0.005 g, 0.010 g, 0.020 g, and 0.050 g, respectively. The removal efficiency of the PB/silica HOM nanocomposites toward heavy metals and pesticides in comparison with the previously reported data are represented in Tables 3 and 4, respectively. The results indicated that the fabricated PB/silica HOM nanocomposites showed good removal efficiency against several heavy metals and pesticides. However, more work is needed to be more efficient.

Conclusion

PB/silica HOM nanocomposites were synthesized based on a simple one-pot method. The PB/silica HOM nanocomposites had high efficiency in the removal of inorganic and organic pollutants from aqueous solutions. Remarkably, it was found that the RE % were 59.97%, 97.33%, 65.39%, 99.4%, 23.14%, 39.60%for Cd(II), Cu(II), Fe(II), Pb(II), Mn(II), and Cr(IV), respectively. Also, the developed nanocomposite showed RE% toward several pesticides to be 94.80%, 89.14%, 100%, 44.55%, 9.52%, 71.43%, 65.96%, 35.64, 35.11% for diazinon, parathion methyl, malathion, parathion ethyl, epoxide, DDE, dieldrin and aldrin, respectively. In addition, 5.71%, 85.50%, and 8.91% removal efficiencies were demonstrated for TS, TDS, TSS, and EC, respectively. Future studies will be conducted to optimize the adsorption process for each contaminant from aqueous solutions and water matrices as well as to prove the adsorption mechanism of contaminants removal from water using different techniques such as FTIR and electron microscopy.

Acknowledgements The authors acknowledge Analytical Chemistry Unit (ACAL) for the use of all equipment throughout this work.

Author Contributions WAES, AAM, and NAEM contributed to conceptualization and supervision; KA, WAES, AAM, and NAEM contributed to methodology; KA, AAM, and WAES contributed to software, data curation, writing—original draft preparation. Writing—revised form, KA, WAES, AAM, and NAEM. All authors have read and agreed to the published version of the manuscript.

Funding This research received no external funding.

Data availability The authors confirm that the data supporting the findings of this study are available within the article.

Declarations

Conflicts of interest The authors declare no conflicts of interest.

References

Abukhadra MR et al (2022a) Insight into the adsorption properties of β-Cyclodextrin/zeolite: a structure for effective removal of Cd^{2+}, PO_4^{3-}, and methyl parathion; kinetics and advanced equilibrium studies. J Inorg Organomet Polym Mater 32(12):4664–4678

Abukhadra MR, Saad I, Othman SI, Katowah DF, Ajarem JS, Alqarni SA, Allam AA, Al Zoubi W et al (2022b) Characterization of Fe0@chitosan/cellulose structure as effective green adsorbent

for methyl parathion, malachite green, and levofloxacin removal: experimental and theoretical studies. J Mol Liq 368:120730
Acar FN, Eren Z (2006) Removal of Cu(II) ions by activated poplar sawdust (Samsun clone) from aqueous solutions. J Hazard Mater 137(2):909–914
Adekunle AS, Farah AM, Pillay J, Ozoemena KI, Mamba BB, Agboola BO (2012) Electrocatalytic properties of prussian blue nanoparticles supported on poly(m-aminobenzenesulphonic acid)-functionalised single-walled carbon nanotubes towards the detection of dopamine. Colloids and surfaces. B, Biointerfaces 95:186–194
Agency, U.S.E.P. (2008) National primary drinking water regulations. US EPA, Office of Water
Agency, U.S.E.P. (2011) Source water assessment. US EPA, Office of Water
Ahmadian M, Anbia M (2021) Synthesis of spherical SBA-15 by poly (vinyl alcohol)/ Hydroxyl-terminated polybutadiene supermicelles as co-surfactant and its application for removal of diazinon from aqueous solution. Environ Technol Innov 24:101899
Alimohammadi V, Sedighi M, Jabbari E (2017) Experimental study on efficient removal of total iron from wastewater using magnetic-modified multi-walled carbon nanotubes. Ecol Eng 102:90–97
Alrefaee S et al (2023) Adsorption and effective removal of organophosphorus pesticides from aqueous solution via novel metal-organic framework: adsorption isotherms, kinetics, and optimization via Box–Behnken design. J Mol Liq. https://doi.org/10.1016/j.molliq.2023.122206
Alsulami QA, Hussein MA, Alsheheri SZ, Elshehy EA, El-Said WA (2022) Unexpected ultrafast and high adsorption performance of Ag(I) and Hg(II) ions from multiple aqueous solutions using microporous functional silica-polymer sponge-like composite. J Market Res 17:2000–2013
Armaghan M, Amini MM (2017) Adsorption of diazinon and fenitrothion on nanocrystalline magnesium oxides. Arab J Chem 10(1):91–99
Azouaou N, Sadaoui Z, Djaafri A, Mokaddem H (2010) Adsorption of cadmium from aqueous solution onto untreated coffee grounds: equilibrium, kinetics and thermodynamics. J Hazard Mater 184:126–134
Baharum NA, Nasir HM, Ishak MY, Isa NM, Hassan MA, Aris AZ (2020) Highly efficient removal of diazinon pesticide from aqueous solutions by using coconut shell-modified biochar. Arab J Chem 13(7):6106–6121
Bakka A, Ait Taleb M, Nabil S, Laknifli A, Rachid M, Abdeljalil B, Bakiz B, Diane Y (2018) Patellidae shells waste as a biosorbent for the removal of aldrin pesticide from aqueous solutions. J Eng Sci Technol 13:925–942
Bin Jusoh A, Cheng WH, Low WM, Nora'aini A, Noor MM (2005) Study on the removal of iron and manganese in groundwater by granular activated carbon. Desalination 182(1):347–353
Ching S, Mohd Suffian Y, Aziz H, Umar M (2011) Influence of impregnation ratio on coffee ground activated carbon as landfill leachate adsorbent for removal of total iron and orthophosphate. Desalination 279:225–234
Cui L, Zhu J, Meng X, Yin H, Pan X, Ai S (2012) Controlled chitosan coated Prussian blue nanoparticles with the mixture of graphene nanosheets and carbon nanoshperes as a redox mediator for the electrochemical oxidation of nitrite. Sens Actuators, B Chem 161:641–647
Dehghani MH et al (2021) Process optimization and enhancement of pesticide adsorption by porous adsorbents by regression analysis and parametric modelling. Sci Rep 11(1):11719
El Bakouri H, Usero J, Morillo J, Ouassini A (2009) Adsorptive features of acid-treated olive stones for drin pesticides: equilibrium, kinetic and thermodynamic modeling studies. Bioresour Technol 100(18):4147–4155
El-Din AFT, El-Khouly ME, Elshehy EA, Atia AA, El-Said WA (2018) Cellulose acetate assisted synthesis of worm-shaped mesopores of MgP ion-exchanger for cesium ions removal from seawater. Micropor Mesopor Mater 265:211–218
El-Said WA, El-Khouly ME, Ali MH, Rashad RT, Elshehy EA, Al-Bogami AS (2018) Synthesis of mesoporous silica-polymer composite for the chloridazon pesticide removal from aqueous media. J Environ Chem Eng 6:2214–2221
Farah A, Thema F, Dikio E (2012a) Electrochemical detection of hydrogen peroxide based on graphene oxide/Prussian blue modified glassy carbon electrode. Int J Electrochem Sci 7:5069–5083
Farah A, Shooto ND, Thema FT, Modise JS, Dikio ED (2012b) Fabrication of prussian blue/multi-walled carbon nanotubes modified glassy carbon electrode for electrochemical detection of hydrogen peroxide. Int J Electrochem Sci 7:4302–4313
Farghali RA, Sobhi M, Gaber SE, Ibrahim H, Elshehy EA (2020) Adsorption of organochlorine pesticides on modified porous Al_30/bentonite: kinetic and thermodynamic studies. Arab J Chem 13(8):6730–6740
Feng S, Li X, Ma F, Liu R, Guanglei Fu, Xing S, Yue X (2016) Prussian blue functionalized microcapsules for effective removal of Cesium in water environment. RSC Adv 6:34399–34410
Fialova K, Motlochova M, Cermakova L, Novotna K, Bacova J, Rousar T, Subrt J, Pivokonsky M (2023) Removal of manganese by adsorption onto newly synthesized TiO_2-based adsorbent during drinking water treatment. Environ Technol 44(9):1322–1333
Firozjaee T, Mehrdadi N, Baghdadi M, Nabi R (2017) The removal of diazinon from aqueous solution by chitosan/carbon nanotube adsorbent. Desalin Water Treat 79:291–300
Foo KY, Lee LK, Hameed BH (2013) Preparation of banana frond activated carbon by microwave induced activation for the removal of boron and total iron from landfill leachate. Chem Eng J 223:604–610
Gunasekara AS, Rubin AL, Goh KS, Spurlock FC, Tjeerdema RS (2008) Environmental fate and toxicology of carbaryl. Rev Environ Contam Toxicol 196:95–121
Gupta VK, Ali I (2001) Removal of DDD and DDE from wastewater using bagasse fly ash, a sugar industry waste. Water Res 35(1):33–40
Haghighi B, Hamidi H, Gorton L (2010) Electrochemical behavior and application of Prussian blue nanoparticle modified graphite electrode. Sens Actuators, B Chem 147:270–276
Hearon SE, Wang M, Phillips TD (2020) Strong adsorption of dieldrin by parent and processed montmorillonite clays. Environ Toxicol Chem 39(3):517–525
Jang E, Pack SP, Kim I, Chung S (2020) A systematic study of hexavalent chromium adsorption and removal from aqueous environments using chemically functionalized amorphous and mesoporous silica nanoparticles. Sci Rep 10:5558
Kabwadza-Corner P et al (2014) Mechanism of diazinon adsorption on iron modified montmorillonite. Am J Anal Chem 5:70–76
Khalil TE, Elhusseiny AF, El-dissouky A, Ibrahim NM (2019) Functionalized chitosan nanocomposites for removal of toxic Cr (VI) from aqueous solution. React Funct Polym 146:104407
Kim J, Kang J, Um W (2022) Simultaneous removal of cesium and iodate using prussian blue functionalized CoCr layered double hydroxide (PB-LDH). J Environ Chem Eng 10:107477
Köse K, Köse DA (2017) Removal of DDE by exploiting the alcohophobic interactions. Environ Sci Pollut Res Int 24(10):9187–9193
Kumar A, Xagoraraki, Pharmaceuticals I (2010) personal care products and endocrine-disrupting chemicals in U.S. surface and finished drinking waters: a proposed ranking system. Sci Total Environ 408:5972–5989
Li ZF, Chen J, Wang L, Chen K, Nie L, Yao S (2007) Improved electrochemical properties of prussian blue by multi-walled carbon nanotubes. J Electroanal Chem 603:59–66

Lin L, Huang X, Wang L, Tang A (2010) Synthesis, characterization and the electrocatalytic application of prussian blue/titanate nanotubes nanocomposite. Solid State Sci 12(10):1764–1769

Liu H, Qu J, Dai R, Ru J, Wang Z (2007) A biomimetic absorbent for removal of trace level persistent organic pollutants from water. Environ Pollut 147(2):337–342

Liu H, Ru J, Qu J, Dai R, Wang Z, Hu C (2009) Removal of persistent organic pollutants from micro-polluted drinking water by triolein embedded absorbent. Biores Technol 100(12):2995–3002

Liu L, Luo X-B, Ding L, Luo S-L (2019) Application of nanotechnology in the removal of heavy metal from water. In: Luo X, Deng F (eds) Nanomaterials for the removal of pollutants and resource reutilization. Elsevier, pp 83–147

Long M, Jiang H, Li X (2021a) Biosorption of Cu^{2+}, Pb^{2+}, Cd^{2+} and their mixture from aqueous solutions by Michelia figo sawdust. Sci Rep 11:11527

Long X, Chen H, Huang T, Zhang Y, Lu Y, Tan J, Chen R (2021b) Removal of Cd (II) from micro-polluted water by magnetic core-shell Fe_3O_4@ Prussian blue. Molecules 26(9):2497

López E, Soto B, Arias M, Núñez A, Rubinos D, Barral MT (1998) Adsorbent properties of red mud and its use for wastewater treatment. Water Res 32(4):1314–1322

Louis S, Proc. (1999) 1999 Conference on hazardous waste research. 121–130.

Lu LC, Wang CI, Sye WF (2011) Applications of chitosan beads and porous crab shell powder for the removal of 17 organochlorine pesticides (OCPs) in water solution. Carbohyd Polym 83(4):1984–1989

Mac Rae IC (1986) Removal of chlorinated hydrocarbons from water and wastewater by bacterial cells adsorbed to magnetite. Water Res 20(9):1149–1152

Melo DR, Lipsztein JL, de Oliveira CA, Bertelli L (1994) 137Cs internal contamination involving a Brazilian accident, and the efficacy of Prussian Blue treatment. Health Phys 66:245–252

Miao Y, Chen J, Wu X, Miao J (2007) Preparation and characterization of hybrid platinum/Prussian blue nanoparticles. Coll Surfaces a: Physicochem Eng. Asp. 295:135–138

Moreira R, Madeira V, José H, Humeres E (2004) Removal of iron from water using adsorbent carbon. SSTEDS 39:271–285

Naushad M, Alothman ZA, Khan MR (2013) Removal of malathion from aqueous solution using De-Acidite FF-IP resin and determination by UPLC–MS/MS: equilibrium, kinetics and thermodynamics studies. Talanta 115:15–23

Niksirat M, Sadeghi R, Esmaili J (2019) Removal of Mn from aqueous solutions, by activated carbon obtained from tire residuals. SN Appl Sci 1(7):782

Nikzad S, Amooey AA, Alinejad-Mir A (2019) Adsorption of diazinon from aqueous solutions by magnetic guar gum-montmorillonite. Chem Data Collect 20:100187

Ong S-A, Toorisaka E, Hirata M, Hano T (2013) Comparative study on kinetic adsorption of Cu (II), Cd (II) and Ni (II) ions from aqueous solutions using activated sludge and dried sludge. Appl Water Sci 3:321–325

Padmavathy KS, Madhu G, Haseena PV (2016) A study on effects of pH, adsorbent dosage, time, initial concentration and adsorption isotherm study for the removal of hexavalent chromium (Cr (VI)) from wastewater by magnetite nanoparticles. Proced Technol 24:585–594

Pal OR, Vanjara AK (2001) Removal of malathion and butachlor from aqueous solution by clays and organoclays. Sep Purif Technol 24(1):167–172

Qu X, Alvarez PJJ, Li Q (2013) Applications of nanotechnology in water and wastewater treatment. Water Res 47:3931–3946

Rajic N, Stojakovic D, Jevtic S, Zabukovec Logar N, Kovac J, Kaucic V (2009) Removal of aqueous manganese using the natural zeolitic tuff from the Vranjska Banja deposit in Serbia. J Hazard Mater 172(2):1450–1457

Ren T, He P, Niu W, Wu Y, Ai L, Gou X (2013) Synthesis of α-Fe2O3 nanofibers for applications in removal and recovery of Cr(VI) from wastewater. Environ Sci Pollut Res Int 20(1):155–162

Rosales GG, Ávila-Pérez P, Reza-García JO, Cabral-Prieto A, Pérez-Gómez EO (2021) Nanoparticle beads of Chitosan-Ethylene Glycol Diglycidyl Ether/Fe for the removal of Aldrin. J Chem 2021:8421840

Ru J, Liu H, Qu J, Wang A, Dai R (2007) Removal of dieldrin from aqueous solution by a novel triolein-embedded composite adsorbent. J Hazard Mater 141:61–69

Sabbagh N, Tahvildari K, Mehrdad Sharif AA (2021) Application of chitosan-alginate bio composite for adsorption of malathion from wastewater: characterization and response surface methodology. J Contam Hydrol 242:103868

Salimi AH, Shamshiri A, Jaberi E, Bonakdari H, Akhbari A, Delatolla R, Hassanvand MR, Agharazi M et al (2022) Total iron removal from aqueous solution by using modified clinoptilolite. Ain Shams Eng J 13(1):101495

Sanad MMS, Gaber S, El-Aswer E, Farahat M (2023) Graphene-magnetite functionalized diatomite for efficient removal of organochlorine pesticides from aquatic environment. J Environ Manage 330:117145

Sawicki R, Mercier L (2006) Evaluation of mesoporous cyclodextrin-silica nanocomposites for the removal of pesticides from aqueous media. Environ Sci Technol 40(6):1978–1983

Sciban M, Klasnja M, Skrbic B (2008) Adsorption of copper ions from water by modified agricultural by-products. Desalination 229:170–180

Shannon MA, Bohn PW, Elimelech M, Georgiadis JG, Mariñas BJ, Mayes AM (2008) Science and technology for water purification in the coming decades. Nature 452:301–310

Sheikhi ZN, Khajeh M, Oveisi AR, Bohlooli M (2021) Functionalization of an iron-porphyrinic metal–organic framework with Bovine serum albumin for effective removal of organophosphate insecticides. J Mol Liq 343:116974

Shokati Poursani A, Nilchi A, Hassani AH, Shariat M, Nouri J (2015) A novel method for synthesis of nano-γ-Al_2O_3: study of adsorption behavior of chromium, nickel, cadmium and lead ions. Int J Environ Sci Technol 12(6):2003–2014

Shrivas K, Ghosale A, Nirmalkar N, Srivastava A, Singh SK, Shinde SS (2017) Removal of endrin and dieldrin isomeric pesticides through stereoselective adsorption behavior on the graphene oxide-magnetic nanoparticles. Environ Sci Pollut Res Int 24(32):24980–24988

Sprynskyy M, Ligor T, Buszewski B (2008) Clinoptilolite in study of lindane and aldrin sorption processes from water solution. J Hazard Mater 151:570–577

Survey, U.S.G. (2010) Source water-quality assessment (SWQA) program.

Üçer A, Uyanik A, Aygün ŞF (2006) Adsorption of Cu(II), Cd(II), Zn(II), Mn(II) and Fe(III) ions by tannic acid immobilised activated carbon. Sep Purif Technol 47(3):113–118

Uogintė I, Lujanienė G, Mažeika K (2019a) Study of Cu (II), Co (II), Ni (II) and Pb (II) removal from aqueous solutions using magnetic Prussian blue nano-sorbent. J Hazard Mater 369:226–235

Uogintė I, Lujanienė G, Valiulis D (2019) Removal of heavy metals from contaminated water using nano-magnetic Prussian blue based on graphene oxide sorbent. 52(18): pp 85-88.

Víctor-Ortega MD, Ochando-Pulido JM, Martínez-Ferez A (2016) Iron removal and reuse from Fenton-like pretreated olive mill wastewater with novel strong-acid cation exchange resin fixed-bed column. J Ind Eng Chem 36:298–305

Weng C-H, Tsai C-Z, Chu S-H, Sharma YC (2007) Adsorption characteristics of copper (II) onto spent activated clay. Sep Purif Technol 54(2):187–197

Xu D, Zhu K, Zheng X, Xiao R (2015) Poly(ethylene-co-vinyl alcohol) functional nanofiber membranes for the removal of Cr(VI) from water. Ind Eng Chem Res 54:6836–6844

Yousif AM, Atia AA, Zaid OF, Ibrahim IA (2015) efficient and fast adsorption of phosphates and sulphates on prepared modified cellulose. J Dispersion Sci Technol 36:1628–1638

Zadeh M, Daghbandan A, Souraki B (2022) Removal of iron and manganese from groundwater sources using nano-biosorbents. Chem Biol Technol Agric 9:1–14

Zhang Y, Wen Y, Liu Y, Li D, Li J (2004) Functionalization of single-walled carbon nanotubes with Prussian blue. Electrochem Commun 6(11):1180–1184

Zhang J, Li J, Yang F, Zhang B, Yang X (2009) Preparation of Prussian blue@Pt nanoparticles/carbon nanotubes composite material for efficient determination of H_2O_2. Sens Actuators, B Chem 143:373–380

Zhou Y-F, Haynes R (2011) Removal of Pb(II), Cr(III) and Cr(VI) from aqueous solutions using alum-derived water treatment sludge. Water Air Soil Pollut 215:631–643

Zhu W, Wang J, Wu D, Li X, Luo Y, Han C, Ma W, He S (2017) Investigating the heavy metal adsorption of mesoporous silica materials prepared by microwave synthesis. Nanoscale Res Lett 12(1):323